



P. Love<sup>at</sup>, H.J. Lubatti<sup>cg</sup>, R. Luna-Garcia<sup>aj,5</sup>, A.L. Lyon<sup>az</sup>, A.K.A. Maciel<sup>b</sup>, D. Mackin<sup>ce</sup>, P. Mättig<sup>ac</sup>, R. Magaña-Villalba<sup>aj</sup>, P.K. Mal<sup>aw</sup>, S. Malik<sup>bq</sup>, V.L. Malyshev<sup>am</sup>, Y. Maravin<sup>bi</sup>, J. Martínez-Ortega<sup>aj</sup>, R. McCarthy<sup>bw</sup>, C.L. McGivern<sup>bh</sup>, M.M. Meijer<sup>al</sup>, A. Melnitchouk<sup>bp</sup>, L. Mendoza<sup>i</sup>, D. Menezes<sup>bb</sup>, P.G. Mercadante<sup>d</sup>, M. Merkin<sup>ao</sup>, A. Meyer<sup>w</sup>, J. Meyer<sup>z</sup>, N.K. Mondal<sup>af</sup>, T. Moulik<sup>bh</sup>, G.S. Muanza<sup>p</sup>, M. Mulhearn<sup>cf</sup>, O. Mundal<sup>x</sup>, L. Mundim<sup>c</sup>, E. Nagy<sup>p</sup>, M. Naimuddin<sup>ae</sup>, M. Narain<sup>cb</sup>, R. Nayyar<sup>ae</sup>, H.A. Neal<sup>bn</sup>, J.P. Negret<sup>i</sup>, P. Neustroev<sup>aq</sup>, H. Nilsen<sup>y</sup>, H. Nogima<sup>c</sup>, S.F. Novaes<sup>e</sup>, T. Nunnemann<sup>ab</sup>, G. Obrant<sup>aq</sup>, D. Onoprienko<sup>bi</sup>, J. Orduna<sup>aj</sup>, N. Osman<sup>au</sup>, J. Osta<sup>bf</sup>, R. Otec<sup>k</sup>, G.J. Otero y Garzón<sup>a</sup>, M. Owen<sup>av</sup>, M. Padilla<sup>ax</sup>, P. Padley<sup>ce</sup>, M. Pangilinan<sup>cb</sup>, N. Parashar<sup>be</sup>, V. Parihar<sup>cb</sup>, S.-J. Park<sup>z</sup>, S.K. Park<sup>ah</sup>, J. Parsons<sup>bu</sup>, R. Partridge<sup>cb</sup>, N. Parua<sup>bd</sup>, A. Patwa<sup>bx</sup>, B. Penning<sup>az</sup>, M. Perfilov<sup>ao</sup>, K. Peters<sup>av</sup>, Y. Peters<sup>av</sup>, P. Pétróff<sup>q</sup>, R. Piegai<sup>a</sup>, J. Piper<sup>bo</sup>, M.-A. Pleier<sup>bx</sup>, P.L.M. Podesta-Lerma<sup>aj,6</sup>, V.M. Podstavkov<sup>az</sup>, M.-E. Pol<sup>b</sup>, P. Polozov<sup>an</sup>, A.V. Popov<sup>ap</sup>, M. Prewitt<sup>ce</sup>, D. Price<sup>bd</sup>, S. Protopopescu<sup>bx</sup>, J. Qian<sup>bn</sup>, A. Quadt<sup>z</sup>, B. Quinn<sup>bp</sup>, M.S. Rangel<sup>q</sup>, K. Ranjan<sup>ae</sup>, P.N. Ratoff<sup>at</sup>, I. Razumov<sup>ap</sup>, P. Renkel<sup>cd</sup>, P. Rich<sup>av</sup>, M. Rijssenbeek<sup>bw</sup>, I. Ripp-Baudot<sup>t</sup>, F. Rizatdinova<sup>ca</sup>, S. Robinson<sup>au</sup>, M. Rominsky<sup>bz</sup>, C. Royon<sup>s</sup>, P. Rubinov<sup>az</sup>, R. Ruchti<sup>bf</sup>, G. Safronov<sup>an</sup>, G. Sajot<sup>o</sup>, A. Sánchez-Hernández<sup>aj</sup>, M.P. Sanders<sup>ab</sup>, B. Sanghi<sup>az</sup>, G. Savage<sup>az</sup>, L. Sawyer<sup>bj</sup>, T. Scanlon<sup>au</sup>, D. Schaile<sup>ab</sup>, R.D. Schamberger<sup>bw</sup>, Y. Scheglov<sup>aq</sup>, H. Schellman<sup>bc</sup>, T. Schliephake<sup>ac</sup>, S. Schlobohm<sup>cg</sup>, C. Schwanenberger<sup>av</sup>, R. Schwienhorst<sup>bo</sup>, J. Sekaric<sup>bh</sup>, H. Severini<sup>bz</sup>, E. Shabalina<sup>z</sup>, V. Shary<sup>s</sup>, A.A. Shchukin<sup>ap</sup>, R.K. Shivpuri<sup>ae</sup>, V. Simak<sup>k</sup>, V. Sirotenko<sup>az</sup>, P. Skubic<sup>bz</sup>, P. Slattey<sup>bv</sup>, D. Smirnov<sup>bf</sup>, G.R. Snow<sup>bq</sup>, J. Snow<sup>by</sup>, S. Snyder<sup>bx</sup>, S. Söldner-Rembold<sup>av</sup>, L. Sonnenschein<sup>w</sup>, A. Sopczak<sup>at</sup>, M. Sosebee<sup>cc</sup>, K. Soustruznik<sup>j</sup>, B. Spurlock<sup>cc</sup>, J. Stark<sup>o</sup>, V. Stolin<sup>an</sup>, D.A. Stoyanova<sup>ap</sup>, J. Strandberg<sup>bn</sup>, M.A. Strang<sup>bt</sup>, E. Strauss<sup>bw</sup>, M. Strauss<sup>bz</sup>, R. Ströhmer<sup>ab</sup>, D. Strom<sup>ba</sup>, L. Stutte<sup>az</sup>, P. Svoisky<sup>al</sup>, M. Takahashi<sup>av</sup>, A. Tanasijczuk<sup>a</sup>, W. Taylor<sup>f,g</sup>, B. Tiller<sup>ab</sup>, M. Titov<sup>s</sup>, V.V. Tokmenin<sup>am</sup>, D. Tsybychev<sup>bw</sup>, B. Tuchming<sup>s</sup>, C. Tully<sup>bs</sup>, P.M. Tuts<sup>bu</sup>, R. Unalan<sup>bo</sup>, L. Uvarov<sup>aq</sup>, S. Uvarov<sup>aq</sup>, S. Uzunyan<sup>bb</sup>, P.J. van den Berg<sup>ak</sup>, R. Van Kooten<sup>bd</sup>, W.M. van Leeuwen<sup>ak</sup>, N. Varelas<sup>ba</sup>, E.W. Varnes<sup>aw</sup>, I.A. Vasilyev<sup>ap</sup>, P. Verdier<sup>u,v</sup>, L.S. Vertogradov<sup>am</sup>, M. Verzocchi<sup>az</sup>, M. Vesterinen<sup>av</sup>, D. Vilanova<sup>s</sup>, P. Vint<sup>au</sup>, P. Vokac<sup>k</sup>, H.D. Wahl<sup>ay</sup>, M.H.L.S. Wang<sup>bv</sup>, J. Warchol<sup>bf</sup>, G. Watts<sup>cg</sup>, M. Wayne<sup>bf</sup>, G. Weber<sup>aa</sup>, M. Weber<sup>az,7</sup>, M. Wetstein<sup>bk</sup>, A. White<sup>cc</sup>, D. Wicke<sup>aa</sup>, M.R.J. Williams<sup>at</sup>, G.W. Wilson<sup>bh</sup>, S.J. Wimpenny<sup>ax</sup>, M. Wobisch<sup>bj</sup>, D.R. Wood<sup>bm</sup>, T.R. Wyatt<sup>av</sup>, Y. Xie<sup>az</sup>, C. Xu<sup>bn</sup>, S. Yacoub<sup>bc</sup>, R. Yamada<sup>az</sup>, W.-C. Yang<sup>av</sup>, T. Yasuda<sup>az</sup>, Y.A. Yatsunenko<sup>am</sup>, Z. Ye<sup>az</sup>, H. Yin<sup>h</sup>, K. Yip<sup>bx</sup>, H.D. Yoo<sup>cb</sup>, S.W. Youn<sup>az</sup>, J. Yu<sup>cc</sup>, C. Zeitnitz<sup>ac</sup>, S. Zelitch<sup>cf</sup>, T. Zhao<sup>cg</sup>, B. Zhou<sup>bn</sup>, J. Zhu<sup>bw</sup>, M. Zielinski<sup>bv</sup>, D. Zieminska<sup>bd</sup>, L. Zivkovic<sup>bu</sup>, V. Zutshi<sup>bb</sup>, E.G. Zverev<sup>ao</sup>

<sup>a</sup> Universidad de Buenos Aires, Buenos Aires, Argentina

<sup>b</sup> LAFEX, Centro Brasileiro de Pesquisas Físicas, Rio de Janeiro, Brazil

<sup>c</sup> Universidade do Estado do Rio de Janeiro, Rio de Janeiro, Brazil

<sup>d</sup> Universidade Federal do ABC, Santo André, Brazil

<sup>e</sup> Instituto de Física Teórica, Universidade Estadual Paulista, São Paulo, Brazil

<sup>f</sup> Simon Fraser University, Burnaby, British Columbia, Canada

<sup>g</sup> York University, Toronto, Ontario, Canada

<sup>h</sup> University of Science and Technology of China, Hefei, People's Republic of China

<sup>i</sup> Universidad de los Andes, Bogotá, Colombia

<sup>j</sup> Center for Particle Physics, Charles University, Faculty of Mathematics and Physics, Prague, Czech Republic

<sup>k</sup> Czech Technical University in Prague, Prague, Czech Republic

<sup>l</sup> Center for Particle Physics, Institute of Physics, Academy of Sciences of the Czech Republic, Prague, Czech Republic

<sup>m</sup> Universidad San Francisco de Quito, Quito, Ecuador

<sup>n</sup> LPC, Université Blaise Pascal, CNRS/IN2P3, Clermont, France

<sup>o</sup> LPSC, Université Joseph Fourier Grenoble 1, CNRS/IN2P3, Institut National Polytechnique de Grenoble, Grenoble, France

<sup>p</sup> CPPM, Aix-Marseille Université, CNRS/IN2P3, Marseille, France

<sup>q</sup> LAL, Université Paris-Sud, IN2P3/CNRS, Orsay, France

<sup>r</sup> LPNHE, IN2P3/CNRS, Universités Paris VI and VII, Paris, France

<sup>s</sup> CEA, Ifju, SPP, Saclay, France

<sup>t</sup> IPHC, Université de Strasbourg, CNRS/IN2P3, Strasbourg, France

<sup>u</sup> IPNL, Université Lyon 1, CNRS/IN2P3, Villeurbanne, France

<sup>v</sup> Université de Lyon, Lyon, France

<sup>w</sup> III. Physikalisches Institut A, RWTH Aachen University, Aachen, Germany

<sup>x</sup> Physikalisches Institut, Universität Bonn, Bonn, Germany

<sup>y</sup> Physikalisches Institut, Universität Freiburg, Freiburg, Germany

<sup>z</sup> II. Physikalisches Institut, Georg-August-Universität Göttingen, Göttingen, Germany

<sup>aa</sup> Institut für Physik, Universität Mainz, Mainz, Germany

<sup>ab</sup> Ludwig-Maximilians-Universität München, München, Germany

<sup>ac</sup> Fachbereich Physik, University of Wuppertal, Wuppertal, Germany

<sup>ad</sup> Panjab University, Chandigarh, India

<sup>ae</sup> Delhi University, Delhi, India

<sup>af</sup> Tata Institute of Fundamental Research, Mumbai, India

<sup>ag</sup> University College Dublin, Dublin, Ireland

- <sup>ah</sup> Korea Detector Laboratory, Korea University, Seoul, Republic of Korea  
<sup>ai</sup> SungKyunKwan University, Suwon, Republic of Korea  
<sup>aj</sup> CINVESTAV, Mexico City, Mexico  
<sup>ak</sup> FOM-Institute NIKHEF and University of Amsterdam/NIKHEF, Amsterdam, The Netherlands  
<sup>al</sup> Radboud University Nijmegen/NIKHEF, Nijmegen, The Netherlands  
<sup>am</sup> Joint Institute for Nuclear Research, Dubna, Russia  
<sup>an</sup> Institute for Theoretical and Experimental Physics, Moscow, Russia  
<sup>ao</sup> Moscow State University, Moscow, Russia  
<sup>ap</sup> Institute for High Energy Physics, Protvino, Russia  
<sup>aq</sup> Petersburg Nuclear Physics Institute, St. Petersburg, Russia  
<sup>ar</sup> Stockholm University, Stockholm, Sweden  
<sup>as</sup> Uppsala University, Uppsala, Sweden  
<sup>at</sup> Lancaster University, Lancaster, United Kingdom  
<sup>au</sup> Imperial College London, London SW7 2AZ, United Kingdom  
<sup>av</sup> The University of Manchester, Manchester M13 9PL, United Kingdom  
<sup>aw</sup> University of Arizona, Tucson, AZ 85721, USA  
<sup>ax</sup> University of California, Riverside, CA 92521, USA  
<sup>ay</sup> Florida State University, Tallahassee, FL 32306, USA  
<sup>az</sup> Fermi National Accelerator Laboratory, Batavia, IL 60510, USA  
<sup>ba</sup> University of Illinois at Chicago, Chicago, IL 60607, USA  
<sup>bb</sup> Northern Illinois University, DeKalb, IL 60115, USA  
<sup>bc</sup> Northwestern University, Evanston, IL 60208, USA  
<sup>bd</sup> Indiana University, Bloomington, IN 47405, USA  
<sup>be</sup> Purdue University Calumet, Hammond, IN 46323, USA  
<sup>bf</sup> University of Notre Dame, Notre Dame, IN 46556, USA  
<sup>bg</sup> Iowa State University, Ames, IA 50011, USA  
<sup>bh</sup> University of Kansas, Lawrence, KS 66045, USA  
<sup>bi</sup> Kansas State University, Manhattan, KS 66506, USA  
<sup>bj</sup> Louisiana Tech University, Ruston, LA 71272, USA  
<sup>bk</sup> University of Maryland, College Park, MD 20742, USA  
<sup>bl</sup> Boston University, Boston, MA 02215, USA  
<sup>bm</sup> Northeastern University, Boston, MA 02115, USA  
<sup>bn</sup> University of Michigan, Ann Arbor, MI 48109, USA  
<sup>bo</sup> Michigan State University, East Lansing, MI 48824, USA  
<sup>bp</sup> University of Mississippi, University, MS 38677, USA  
<sup>bq</sup> University of Nebraska, Lincoln, NE 68588, USA  
<sup>br</sup> Rutgers University, Piscataway, NJ 08855, USA  
<sup>bs</sup> Princeton University, Princeton, NJ 08544, USA  
<sup>bt</sup> State University of New York, Buffalo, NY 14260, USA  
<sup>bu</sup> Columbia University, New York, NY 10027, USA  
<sup>bv</sup> University of Rochester, Rochester, NY 14627, USA  
<sup>bw</sup> State University of New York, Stony Brook, NY 11794, USA  
<sup>bx</sup> Brookhaven National Laboratory, Upton, NY 11973, USA  
<sup>by</sup> Langston University, Langston, OK 73050, USA  
<sup>bz</sup> University of Oklahoma, Norman, OK 73019, USA  
<sup>ca</sup> Oklahoma State University, Stillwater, OK 74078, USA  
<sup>cb</sup> Brown University, Providence, RI 02912, USA  
<sup>cc</sup> University of Texas, Arlington, TX 76019, USA  
<sup>cd</sup> Southern Methodist University, Dallas, TX 75275, USA  
<sup>ce</sup> Rice University, Houston, TX 77005, USA  
<sup>cf</sup> University of Virginia, Charlottesville, VA 22901, USA  
<sup>cg</sup> University of Washington, Seattle, WA 98195, USA

## ARTICLE INFO

## Article history:

Received 12 January 2010

Received in revised form 9 July 2010

Accepted 7 September 2010

Available online 17 September 2010

Editor: H. Weerts

## Keywords:

Top quark

Differential cross sections

Perturbative QCD

## ABSTRACT

We present a measurement of the differential cross section for  $t\bar{t}$  events produced in  $p\bar{p}$  collisions at  $\sqrt{s} = 1.96$  TeV as a function of the transverse momentum ( $p_T$ ) of the top quark. The selected events contain a high- $p_T$  lepton ( $\ell$ ), a large imbalance in  $p_T$ , four or more jets with at least one candidate for a  $b$  jet, and correspond to  $1 \text{ fb}^{-1}$  of integrated luminosity recorded with the D0 detector. Objects in the event are associated through a constrained kinematic fit to the  $t\bar{t} \rightarrow WbW\bar{b} \rightarrow \ell vbq\bar{q}'\bar{b}$  process. Results from next and next-to-next-to-leading-order perturbative QCD calculations agree with the measured differential cross section. Comparisons are also provided to predictions from Monte Carlo event generators using QCD calculations at different levels of precision.

© 2010 Elsevier B.V. Open access under [CC BY license](#).<sup>1</sup> Visitor from Augustana College, Sioux Falls, SD, USA.<sup>2</sup> Visitor from The University of Liverpool, Liverpool, UK.<sup>3</sup> Visitor from SLAC, Menlo Park, CA, USA.<sup>4</sup> Visitor from ICREA/IFAE, Barcelona, Spain.<sup>5</sup> Visitor from Centro de Investigacion en Computacion – IPN, Mexico City, Mexico.<sup>6</sup> Visitor from ECFM, Universidad Autonoma de Sinaloa, Culiacán, Mexico.<sup>7</sup> Visitor from Universität Bern, Bern, Switzerland.

The transverse momentum ( $p_T$ ) of top quarks in  $t\bar{t}$  events provides a unique window on heavy-quark production at large momentum scales. In the standard model (SM), the lifetime of the top quark is far shorter than the characteristic hadron-formation time of quantum chromodynamics (QCD), which provides access to the properties and kinematics of a “bare” quark, such as mass, charge, spin, and  $p_T$ , that are almost unaffected by bound-state forma-

tion or final-state interactions [1]. The top quark is unique in that it has a mass close to the scale of electroweak symmetry breaking. Detailed studies of the properties of this bare quark beyond the measurement of its total production rate, such as the measurement of its quantum numbers and of its couplings to other SM particles, may indicate whether the top quark plays a privileged role in the symmetry breaking. Focusing on details of the  $t\bar{t}$  production, measurements of differential cross sections in the  $t\bar{t}$  system test perturbative QCD (pQCD) for heavy-quark production and can constrain potential new physics beyond the SM [2], e.g., by measuring the transverse momentum of the top quark [3].

In this Letter, we present a new measurement of the inclusive differential cross section for  $p\bar{p} \rightarrow t\bar{t} + X$  production at  $\sqrt{s} = 1.96$  TeV as a function of the  $p_T$  of the top quark. The measurement is corrected for detector efficiency, acceptance and resolution effects, making it possible to perform direct comparisons with different theoretical predictions. The data were acquired with the D0 detector at the Fermilab Tevatron Collider and correspond to an integrated luminosity of  $\approx 1$  fb $^{-1}$ . This measurement was performed in the  $\ell + \text{jets}$  decay channel of  $t\bar{t} \rightarrow WbW\bar{b} \rightarrow \ell\nu + b\bar{b} + \geq 2$  jets, where  $\ell$  represents an  $e$  or  $\mu$  from the decay of the  $W$  boson or from  $W \rightarrow \tau \rightarrow \ell$ . The dependence of the cross section on the  $p_T$  of the top quark was examined previously using  $\approx 100$  pb $^{-1}$  of Tevatron Run I data at  $\sqrt{s} = 1.8$  TeV [4], where no deviations from the SM were reported.

The D0 detector [5] is equipped with a 2 T solenoidal magnet surrounding silicon-microstrip and scintillating-fiber trackers. These are followed by electromagnetic (EM) and hadronic uranium/liquid argon calorimeters, and a muon spectrometer consisting of 1.8 T iron toroidal magnets and wire chambers and scintillation counters. Electrons are identified as track-matched energy clusters in the EM calorimeter. Muons are identified by matching tracks in the inner tracking detector with those in the muon spectrometer. Jets are reconstructed from calorimeter energies using the Run II iterative seed-based midpoint cone algorithm with a radius of 0.5 [6]. Jets are identified as originating from a  $b$  quark using an artificial neural network ( $b$  NN) which combines several tracking variables [7]. Large missing transverse energy,  $\cancel{E}_T$  (the negative of the vector sum of transverse energies of calorimeter cells, corrected for reconstructed muons) signifies the presence of an energetic neutrino. Events are selected using a three-level trigger system, which has access to tracking, calorimeter, and muon information, and assures that only events with the desired topology or with objects above certain energy thresholds are kept for further analysis.

The analysis uses similar data samples, event selection, and corrections as used in the inclusive  $t\bar{t} \rightarrow \ell + \text{jets}$  cross-section measurements detailed in Ref. [8]. Events accepted by lepton + jets triggers are subject to additional selection criteria including exactly one isolated lepton with  $p_T > 20$  GeV/ $c$  and  $\geq 4$  jets with  $p_T > 20$  GeV/ $c$  and  $|\eta| < 2.5^8$ ; at least one jet must have  $p_T > 40$  GeV/ $c$ . At least one jet is also required to be tagged by the  $b$  NN algorithm. Additionally, we require  $\cancel{E}_T > 20$  GeV (25 GeV) for the  $e + \text{jets}$  ( $\mu + \text{jets}$ ) channel and electrons (muons) with  $|\eta| < 1.1$  (2.0).

Our measurement uses the ALPGEN [9] event generator, with PYTHIA [10] for parton showering, hadronization, and modeling of the underlying event, to simulate the inclusive  $t\bar{t}$  signal. A PYTHIA sample serves as a cross check. The CTEQ6L1 set of parton distribution functions (PDFs) [11] was used with a common fac-

**Table 1**

Expected yields for signal and backgrounds samples and observed event counts in  $e + \text{jets}$  and  $\mu + \text{jets}$  channels.

Sample	$e + \text{jets}$	$\mu + \text{jets}$
$t\bar{t}$	131	108
$W + \text{jets}$	10	15
$Z + \text{jets}$	3.0	3.1
Single top	2.7	2.0
Diboson	1.3	1.3
Multijet	9.0	0.0
Summed prediction	156	130
Total background uncertainty	3.0	2.8
Predicted signal uncertainty	11	9.0
Data	145	141

torization and renormalization scale set to  $\mu = m_t + \sum p_T^{\text{jets}}$  for  $m_t = 170$  GeV/ $c^2$ . Backgrounds are modeled with ALPGEN + PYTHIA for  $W + \text{jets}$  and  $Z + \text{jets}$  production, PYTHIA for diboson ( $WW$ ,  $WZ$ , and  $ZZ$ ) production, and COMPHEP [12] for single top-quark production. The detector response is simulated using GEANT [13]. The simulated  $t\bar{t}$  signal is normalized to the cross section measured by a dedicated likelihood fit in the same final state using the same event selections (including the  $b$ -tagging requirement) and data as Ref. [8], namely to  $8.46_{-0.97}^{+1.09}$  pb at a top-quark mass  $m_t = 170$  GeV/ $c^2$  (in good agreement with the value extracted in this study by integrating the differential cross section). The diboson and single top-quark backgrounds are normalized to their SM predictions,  $Z + \text{jets}$  to the prediction from next-to-leading-order (NLO) pQCD, and  $W + \text{jets}$  such that the predicted number of events matches the data before applying  $b$  tagging.

The small multijet background, in which a jet is misidentified as an isolated lepton, is non-negligible only in the  $e + \text{jets}$  channel. Its rate is estimated from data using the large difference in the probability of electromagnetic showers of real electrons or misidentified jets to satisfy the electron selection criteria. The details of the sample composition and the observed yields before and after requiring the jets to be tagged as  $b$ -jet are presented in Table 1.

The selection yields 145 and 141 events in the  $e + \text{jets}$  and  $\mu + \text{jets}$  decay channels, respectively. The measured  $t\bar{t}$  signal fraction is 0.79, indicating that this sample is suitable for detailed studies of  $t\bar{t}$  production. A constrained kinematic fit to the  $t\bar{t}$  final state, which takes into account the unreconstructed neutrino and finite experimental resolution, is used to associate leptons and jets with individual top quarks [14,15]. The fit assumes equal masses for the two reconstructed top quarks and the two reconstructed  $W$  boson masses are constrained to 80.4 GeV/ $c^2$ . All possible permutations of objects needed to produce the  $t\bar{t}$  system are considered, and the solution of fitted leptonic and hadronic top-quark four-momenta with the smallest  $\chi^2$  (the goodness of the fit) is selected for further analysis. The  $b$ -jet assignment information is not used in the selection of the best permutation to avoid the associated efficiency loss. The effects of possibly selecting a wrong permutation when choosing the one with the best  $\chi^2$  are taken into account in the corrections of the measurement to the parton level. The solution with the best (second best)  $\chi^2$  corresponds to the correct assignment of the quarks from the decay of the  $t\bar{t}$  pair in 48% (17%) of events.

The reconstructed top-quark mass ( $m_t$ ) from the best fit in data, simulated  $t\bar{t}$  signal, and background is shown in Fig. 1. There is good agreement between the data and the sum of signal and background expectations in terms of the shape, resolution, and mean of the distribution in  $m_t$  ( $\chi^2/\text{NDF} = 1.28$ ). The  $p_T$  spectrum of the top quark (for leptonic and hadronic entries) in data, together with predicted signal and background, is shown in Fig. 2 for the best solution but now refitted with a top-quark mass fixed to 170 GeV/ $c^2$

<sup>8</sup> Pseudorapidity is defined as  $\eta = -\ln \tan(\theta/2)$  where  $\theta$  is the angle measured with respect to the proton beam coinciding with the positive  $z$  axis of a right-handed coordinate system at the center of the detector.

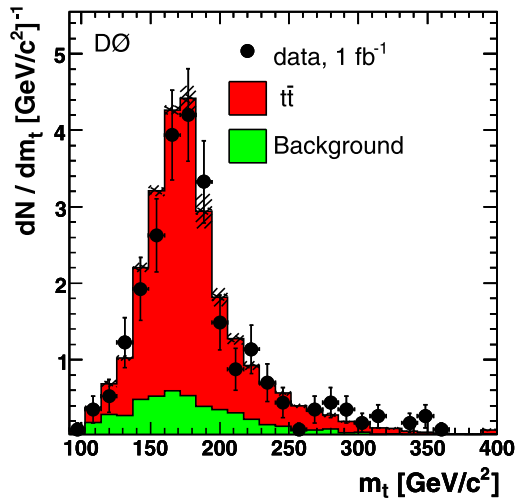


Fig. 1. The reconstructed top-quark mass compared with expectation. Hashed areas represent statistical and jet energy calibration uncertainties on the prediction.

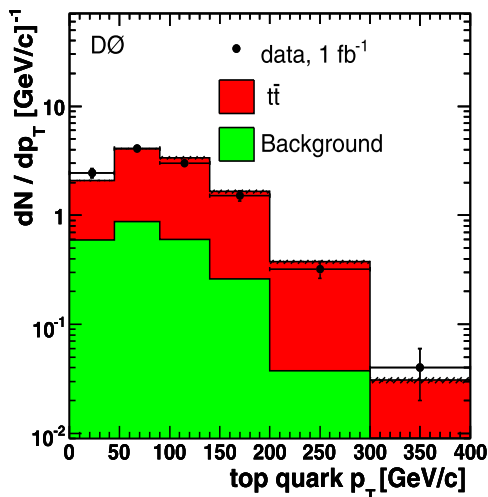


Fig. 2. The  $p_T$  spectrum of top quarks (two entries per event) compared with expectation. Hashed areas represent statistical and jet energy calibration uncertainties on the prediction.

(the value used in the inclusive cross section measurement [8]) to improve resolution. To obtain a background-subtracted data spectrum, the signal purity is fitted using signal and background contributions as a function of  $p_T$ , and applied as a smooth multiplicative factor to the data. The result is the background-corrected distribution shown as a solid line in Fig. 3.

The reconstructed  $p_T$  spectrum is subsequently corrected for effects of finite experimental resolution, based on a regularized unfolding method [16,17] using a migration matrix between the reconstructed and parton  $p_T$  derived from simulation. The size of the  $p_T$  bins was chosen based on the requirement that the purity (the fraction of parton-level events which are reconstructed in the correct  $p_T$  range) is  $> 50\%$ , as shown in Table 2. This also results in  $p_T$  bins which are larger than the experimental resolution for the top quark  $p_T$ . The correlation between reconstructed and correct  $p_T$  is  $> 80\%$ . Fig. 3 compares the reconstructed and corrected results as a function of the  $p_T$  of the top quark. The dependence of the unfolding on the parton spectrum shape in the migration matrix is tested by reweighting the distribution with arbitrary functions. Shape variations of  $\approx 20\%$  induce 2–6% changes in the differential cross section. A correction for acceptance from

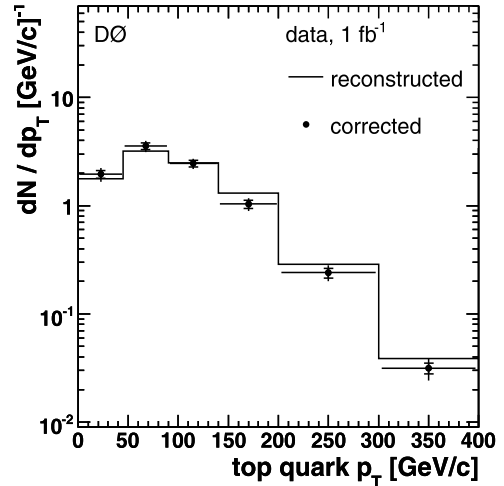


Fig. 3. Comparison between the background-subtracted reconstructed top-quark  $p_T$  spectrum and the one corrected for the effects of finite experimental resolution (two entries per event). Inner and outer error bars represent the statistical and total (statistical and systematic added in quadrature) uncertainties, respectively.

Table 2

The migration matrix between the reconstructed (rows) and parton (columns) top-quark  $p_T$  derived from ALPGEN  $t\bar{t}$  events passed through full detector simulation. The matrix indicates the fraction of events migrated from a given parton bin to the reconstructed bins. The binning used for correlating reconstructed and parton levels of  $p_T$  are given at the left and top, respectively. Results in bold print are for diagonal terms.

$p_T$ (GeV/c)	0–45	45–90	90–140	140–200	200–300	300–400
0–45	<b>0.530</b>	0.162	0.062	0.020	0.003	0.000
45–90	0.344	<b>0.578</b>	0.227	0.072	0.021	0.000
90–140	0.103	0.228	<b>0.560</b>	0.223	0.055	0.031
140–200	0.019	0.029	0.145	<b>0.581</b>	0.232	0.071
200–300	0.002	0.002	0.006	0.103	<b>0.650</b>	0.363
300–400	0.000	0.000	0.000	0.001	0.038	<b>0.535</b>

the dependence of the spectrum on kinematic restrictions of reconstructed quantities is applied to the unfolded distributions.

The measured differential cross section as a function of the  $p_T$  of the top quark (using for each event the two measurements obtained from the leptonic and hadronic top quark decays),  $d\sigma/dp_T$ , is shown in Fig. 4 and tabulated in Table 3 together with the NLO pQCD prediction [18,19]. The statistical uncertainties are estimated by performing 1000 pseudo-experiments where, in each experiment, the background-corrected spectrum is allowed to vary according to Poisson statistics and is then unfolded using the regularized migration matrix (Table 2). The largest experimental uncertainties affecting the shape of the  $p_T$  distribution include jet energy calibration in data and in simulation (1.5–5.0%), jet reconstruction efficiency (0.7–3.5%), and jet energy resolution ( $\approx 0.5\%$ ). The residual dependence of the unfolded result on the top-quark mass is 2–6% for  $m_t$  in the 170–175  $\text{GeV}/c^2$  range. This additional uncertainty does not need to be considered for comparisons with models in which  $m_t$  is set to 170  $\text{GeV}/c^2$ . For the main background sources,  $W/Z$  + jets, we have also considered the variations of the background shape caused by uncertainties in the  $k$ -factors and in additional scale factors for heavy-flavor jets. Other systematic uncertainties [8] account for uncertainties in the modeling of the signal, estimated from the difference between ALPGEN and PYTHIA, for uncertainties in the PDFs and in the  $b$ -quark fragmentation. The uncertainty on the integrated luminosity is 6.1%. The systematic uncertainties quoted in the following combine the uncertainty on the normalization (independent of  $p_T$ ) with the shape-dependent systematics. The total correlated systematic uncertainty is 9.6% (in-

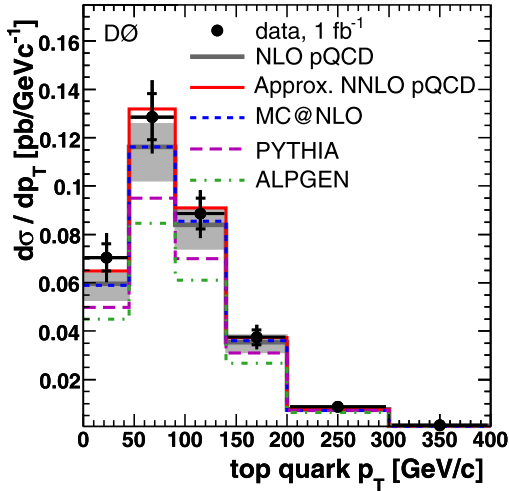


**Fig. 4.** Inclusive  $d\sigma/dp_T$  for  $t\bar{t}$  production (two entries per event) in data (points) compared with expectations from NLO pQCD (solid lines), from an approximate NNLO pQCD calculation, and for several event generators (dashed and dot-dashed lines). The gray band encompasses uncertainties on the pQCD scale and parton distribution functions. Inner and outer error bars represent the statistical and total (statistical and systematic added in quadrature) uncertainties, respectively.

**Table 3**

Inclusive differential cross section  $d\sigma/dp_T$  for  $t\bar{t}$  production at  $\sqrt{s} = 1.96$  TeV and  $m_t = 170$  GeV/ $c^2$ . There are two entries per event, with the total normalized to the  $t\bar{t}$  production cross section. In addition to total systematic uncertainties on the shape in  $p_T$  in each bin, there is a  $p_T$ -independent systematic uncertainty of 9.6% that is not included in the table.

$p_T$ (GeV/ $c$ )	$\langle p_T \rangle$ (GeV/ $c$ )	Cross section (fb/GeV)	Stat. unc. (fb/GeV)	Shape sys. unc. (fb/GeV)	NLO pQCD (fb/GeV)
0–45	29	70	11	5	59.6
45–90	68	130	20	10	116
90–140	113	89	13	6	83.8
140–200	165	37	6	3	35.6
200–300	233	8.7	1.7	0.7	7.72
300–400	329	1.1	0.3	0.1	0.814
$\sigma_{t\bar{t}}$ (pb)		8.31	1.28		7.54

cluding the uncertainty on luminosity) and the total systematic uncertainty on the cross section, integrating over  $p_T$ , is 10.7%.

Results from NLO pQCD [18,19] calculations obtained using CTEQ61 [20] PDFs (using the scale  $\mu = m_t = 170$  GeV/ $c^2$ ) are overlaid on the measured differential cross section in Fig. 4. Also shown are results from an approximate next-to-NLO (NNLO) pQCD calculation [21] computed using MSTW2008 NLO PDFs [22] and same scales choices as the NLO result, and from the MC@NLO [23] (using CTEQ61 PDFs), ALPGEN, and PYTHIA event generators. The QCD scale uncertainty was evaluated for the NLO pQCD calculation [18, 19] by varying  $\mu = m_t = 170$  GeV/ $c^2$  by factors of 2 and 1/2, and the PDF uncertainty by the approximate NNLO code [21]. The total uncertainty is  $< 4\%$  with only a small ( $< 1\%$ ) shape variation. A comparison of the ratio of  $d\sigma/dp_T$  relative to a NLO pQCD calculation is shown in Fig. 5. The NLO pQCD calculations agree with the measured cross section, however, results from ALPGEN (PYTHIA) have a normalization shift of about 45% (30%) with respect to data. A shape comparison of the ratio of  $(1/\sigma)d\sigma/dp_T$  relative to NLO pQCD is shown in Fig. 6. All of the calculations reproduce the observed shape. The  $\chi^2$  and corresponding  $\chi^2$  probabilities [24] for the comparisons in Figs. 5 and 6 of predictions to data are given in Table 4.

In conclusion, we have presented a  $1 \text{ fb}^{-1}$  measurement of the differential cross section of the top-quark  $p_T$  for  $t\bar{t}$  production

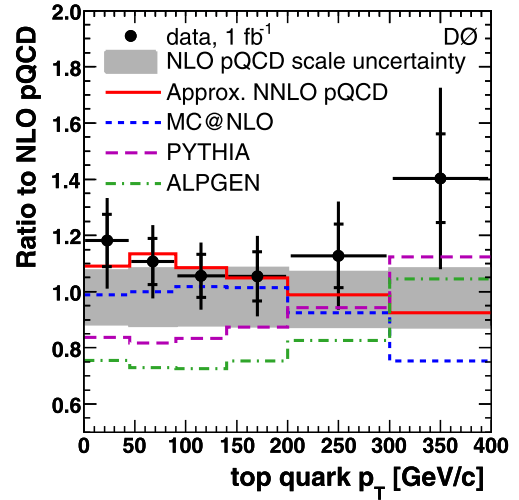


**Fig. 5.** Ratio of  $d\sigma/dp_T$  for top quarks in  $t\bar{t}$  production (two entries per event) to the expectation from NLO pQCD. The gray band encompasses uncertainties on the scale of pQCD and parton distribution functions. Also shown are ratios relative to NLO pQCD for an approximate NNLO pQCD calculation and of predictions for several event generators. Inner and outer error bars represent statistical and total (statistical and systematic added in quadrature) uncertainties, respectively.

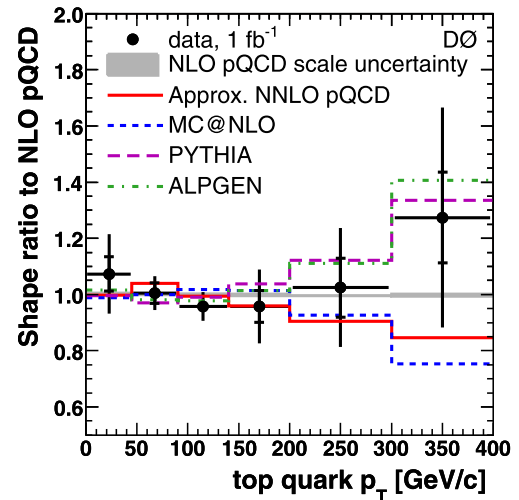


**Fig. 6.** Ratio of  $(1/\sigma)d\sigma/dp_T$  for top quarks in  $t\bar{t}$  production (two entries per event) to the expectation from NLO pQCD. The gray band encompasses uncertainties on the scale of pQCD and parton distribution functions. Also shown are ratios relative to NLO pQCD for an approximate NNLO pQCD calculation and of predictions for several event generators. Inner and outer error bars represent statistical and total (statistical and systematic added in quadrature) uncertainties, respectively.

**Table 4**

The  $\chi^2/\text{NDF}$  and  $\chi^2$  probability for comparisons between the measured data and predictions using correlated (uncorrelated) uncertainties for the absolute (shape) comparison.

Prediction	Absolute		Shape	
	$\chi^2/\text{NDF}$	Prob.	$\chi^2/\text{NDF}$	Prob.
NLO pQCD	0.695	0.653	0.315	0.904
Approx. NNLO pQCD	0.521	0.793	0.497	0.779
MC@NLO	1.22	0.295	0.777	0.566
PYTHIA	2.61	0.0157	0.352	0.881
ALPGEN	5.04	$3.54 \times 10^{-5}$	0.204	0.961

in the  $\ell + \text{jets}$  channel using  $p\bar{p}$  collisions at  $\sqrt{s} = 1.96$  TeV. Results from NLO and NNLO pQCD calculations and from the MC@NLO

event generator agree with the normalization and shape of the measured cross section. Results from ALPGEN + PYTHIA and PYTHIA describe the shape of the data distribution, but not its normalization.

### Acknowledgements

We thank the staffs at Fermilab and collaborating institutions, and acknowledge support from the DOE and NSF (USA); CEA and CNRS/IN2P3 (France); FASI, Rosatom and RFBR (Russia); CNPq, FAPERJ, FAPESP and FUNDUNESP (Brazil); DAE and DST (India); Colciencias (Colombia); CONACyT (Mexico); KRF and KOSEF (Korea); CONICET and UBACyT (Argentina); FOM (The Netherlands); STFC and the Royal Society (United Kingdom); MSMT and GACR (Czech Republic); CRC Program, CFI, NSERC and WestGrid Project (Canada); BMBF and DFG (Germany); SFI (Ireland); The Swedish Research Council (Sweden); and CAS and CNSF (China).

### References

- [1] I. Bigi, et al., Phys. Lett. B 181 (1986) 157.
- [2] C.T. Hill, S.J. Parke, Phys. Rev. D 49 (1994) 4454.
- [3] D. Atwood, et al., Phys. Rev. D 52 (1995) 6264.
- [4] T. Affolder, et al., CDF Collaboration, Phys. Rev. Lett. 87 (2001) 102001; B. Abbott, et al., D0 Collaboration, Phys. Rev. D 58 (1998) 052001.
- [5] V.M. Abazov, et al., D0 Collaboration, Nucl. Instrum. Methods Phys. Res. A 565 (2006) 463.
- [6] G.C. Blazey, et al., in: U. Baur, R.K. Ellis, D. Zeppenfeld (Eds.), Proceedings of the Workshop: QCD and Weak Boson Physics in Run II, 2000, Fermilab-Pub-00/297.
- [7] V.M. Abazov, et al., D0 Collaboration, Nucl. Instrum. Methods Phys. Res. A 620 (2010) 400.
- [8] V.M. Abazov, et al., D0 Collaboration, Phys. Rev. D 80 (2009) 071102 (RC).
- [9] M.L. Mangano, et al., J. High Energy Phys. 0307 (2003) 001.
- [10] T. Sjöstrand, et al., Comput. Phys. Commun. 135 (2001) 238; R. Field, R.C. Group, arXiv:hep-ph/0510198.
- [11] J. Pumplin, et al., J. High Energy Phys. 0207 (2002) 012.
- [12] E.E. Boos, et al., Phys. At. Nucl. 69 (2006) 1317; E.E. Boos, et al., Yad. Fiz. 69 (2006) 1352.
- [13] R. Brun, F. Carminati, CERN Program Library Long Writeup W5013, 1993 (unpublished).
- [14] V.M. Abazov, et al., D0 Collaboration, Phys. Rev. D 75 (2007) 092001.
- [15] S. Snyder, Ph.D. thesis, State University of New York at Stony Brook, 1995, Institution Report No. FERMILAB-THESIS-1995-27.
- [16] A. Hoecker, V. Kartvelishvili, Nucl. Instrum. Methods Phys. Res. A 372 (1996) 469.
- [17] V. Kartvelishvili, <http://www.lancs.ac.uk/users/spc/staff/kartvelishvili.htm>.
- [18] M. Mangano, P. Nason, G. Ridolfi, Nucl. Phys. B 373 (1992) 295.
- [19] P. Nason, S. Dawson, R.K. Ellis, Nucl. Phys. B 327 (1989) 49; P. Nason, S. Dawson, R.K. Ellis, Nucl. Phys. B 335 (1990) 260 (Erratum).
- [20] D. Stump, et al., J. High Energy Phys. 0310 (2003) 046.
- [21] N. Kidonakis, R. Vogt, Phys. Rev. D 78 (2008) 074005.
- [22] A.D. Martin, W.J. Stirling, R.S. Thorne, G. Watt, Eur. Phys. J. C 63 (2009) 189.
- [23] S. Frixione, B.R. Webber, J. High Energy Phys. 0206 (2002) 029; S. Frixione, P. Nason, B.R. Webber, J. High Energy Phys. 0308 (2003) 007.
- [24] N.D. Gagunashvili, Nucl. Instrum. Methods Phys. Res. A 596 (2008) 439.